Investigation on the Effects of Different Incident Angle of Sarpol-e Zahab Earthquake Ground Motions on an Embankment Dam

Mohammad Davoodi[1*] and Fariborz Sanjari[2]

1. Associate Professor, Geotechnical Engineering Research Center, International Institute of Earthquake Engineering and Seismology (IIEES), Tehran, Iran,
* Corresponding Author; email: m-davood@iiees.ac.ir
2. Ph.D. Candidate, International Institute of Earthquake Engineering and Seismology (IIEES), Tehran, Iran

Received: 23/04/2018
Accepted: 18/11/2018

ABSTRACT

One of the most important challenges in analysis of non-ordinary structures is the critical angle of incidence of earthquake ground motions. To accommodate these directional effects, several procedures and combination rules have been proposed. The major limitations of these methods are that they are restricted to elastic analyses, rarely considered near-fault earthquakes and are almost related to the building structures or bridges. The main objective of this work is to assess the influence of incident angle of ground motions on several engineering demand parameters (EDPs) of an embankment dam under Sarpol-e Zahab earthquake. To achieve this goal, after selecting proper ground motions, the as-recorded horizontal components (two orthogonal) were rotated to: fault-normal/parallel direction, principal direction, direction related to GMrotIpp (NGA relationships) and maximum direction of response history analysis of two degree of freedom system (MSD). In the next step, a typical embankment dam in the earthquake-affected areas was modeled using the shear beam method. The model was excited by as-recorded motions with various directions in the range of 0-360 degrees with a step of 10 degrees and all four above-mentioned reference axes directions. Numerous equivalent linear analyses were carried out to obtain the critical angles of excitation that leads to maximum responses. The analyses results showed that the critical orientations of ground motions depend on: input motions, structure characteristics and EDPs.

Keywords:
Sarpol-e Zahab Earthquake; Reference axes; Embankment; Critical orientation; Incident angle

1. Introduction

In designing and analyzing of structures against earthquake forces, one of the important challenges is the lack of sufficient information about the incident angle of earthquake ground motion. Due to uncertainties such as the location of future earthquakes, the source, path and the site characteristics considering different directions for an earthquake seems to be logical. To investigate these effects, a lot of research has been done and 100% + 30%, 100% + 40%, SRSS and CQC3 combination rules have been proposed [1-6].

These approaches are applicable in the range of linear analysis and are used in response spectrum method. Parametric analysis is required to consider nonlinear behavior of the structures. In this approach, structures are analyzed using different incident angles of ground motion records and responses are calculated. The direction leading to the maximum

response is known as a critical direction. In these methods, regardless of the reference axes, as-recorded ground motions are generally used [7-13].

Recorded accelerations depend on the orientation of the sensors as installed in the field, and by rotating the sensors, different accelerations are recorded for a specific ground motion. Considering that the orientation of sensors is random compared to the orientation of the structures and causative fault, it is necessary to consider the definite reference axes for earthquake records. Meanwhile, Ground Motion Prediction Equations (GMPEs) of NGA project are based on the GMRotI50 (Geometric Mean Independent of period and sensor orientations) [14] and in the ASCE/SEI 7 standard, after 2010 version, the MSD (Maximum Spectral Demand) and FN/FP (Fault Normal/Fault Parallel) directions have been used [15]. By reviewing the literature, all reference axes of earthquake ground motions can be categorized as follows:

1) As-recorded ground motion records (using recorded ground motion without rotating its axes)
2) Principal axes (PD)
3) Fault Normal and Fault Parallel direction (FN/FP)
4) Geometric Mean Independent of period and sensor orientations (GMRotIpp)
5) Maximum Spectral Demand (MSD)

Penzien and Watabe [16] defined an orthogonal set of principal axes along which the variances of earthquake ground motion components have maximum, minimum and intermediate values, while covariances are equal to zero. The involved procedure is similar to finding the principal directions of stresses in the classical strength of materials. The paper suggested the moving window to calculate variances of components and showed that for the window of highest intensity, the principal direction is toward earthquake epicenter [16-18]. Related researches investigated the response of structures subjected to principal component and various rotated ground motion records. Results of the analysis indicated that the responses due to principal components is higher than as-recorded accelerations, while the critical responses may occur in different directions [19].

Typically, ground motions that are recorded in stations less than 20 km away from the epicenter are known as the near-fault earthquake, however, the important characteristics and parameters of this type of earthquake should be taken into account [20]. Characteristics of near-fault earthquakes are directly related to the source mechanism, direction of fault rupture and location of the station with respect to the epicenter. The most important distinguishing features of near-fault earthquakes is the forward directivity. This phenomenon results in the accumulation of seismic energy in the fault normal direction and causes pulse-like motions [21-27]. Concerning this issue, it is assumed that rotating of the ground motion components in the direction of FN/FP is a conservative method and suitable for the seismic evaluation of structures in the near-fault region. Therefore, the ASCE/SEI 7 Regulation states that in the near-fault region ground motion acceleration should be rotated in the FN/FP direction. While research shows that this direction does not always lead to a maximum response of structures [28-30].

The geometric mean of the response spectra of two horizontal ground motion components, which is commonly used as a response variable in predicting strong ground motion, depends on the orientation of the sensors. This results in different ground-motion intensity for the specific ground motion. This dependency is more pronounced in a strongly correlated motion such as that occurs in periods of 1 second or longer. Boore et al. [31] introduced two orientation independent measurements as GMRotIpp and GMRotDpp. In these nomenclatures "GM" stands for geometric mean, "Rot" indicates rotations over all non-redundant angles, "D" and "I" shows period dependent and period independent respectively, and "pp" stands for statistical percent percentile. Although the GMRotDpp measurement is independent of the orientation of the sensor, its important shortcoming is the dependence on the oscillator period. This means that GMRotIpp measurement leads to one definite angle for each ground motion acceleration. Therefore, the ground motion acceleration after rotating by this angle can be used in time history analysis.

The USGS seismic hazard maps and attenuation relationships used in regulations prior to NEHRP 2009 were based on probabilistic seismic hazard analysis and geometric mean (GM, GMRotI50). NEHRP 2009 provision utilizes maximum spectral

demand (MSD) direction and deterministic seismic hazard analysis in the near-fault regions. Therefore, according to Baker and Cornell [32], when using the spectral acceleration, the value of the standard deviation must be taken into account. Because if the maximum value is defined by the mean value plus the standard deviation, if the GMRotI50 direction is used instead of as-recorded ground motion, due to the lower standard deviation of the GMRotI50, the probability of the earthquakes with a long return period is less predicted.

The ASCE / SEI-7-10 uses the Maximum spectral demand (MSD) to provide the site specific spectrum. The MSD direction is corresponding to the maximum spectral response of the single degree of freedom oscillator. The SDOF oscillator with 5% damping and period of T_i is subjected to each horizontal component and responses is calculated as $A(t, T_i, x)$ and $A(t, T_i, y)$ by drawing the $A(t, T_i, x)$-$A(t, T_i, y)$ graph according to Section 3.3, the orientation corresponding to the point on the orbit farthest from the origin is identified as MSD. The mean value of the MSD is systematically greater than the GM and their ratio depends on oscillator period and is in the range of 1.1 to 1.5 [33-34].

The researches on reference axes of earthquake ground motions have focused on concrete and steel structures and no investigation has been carried out on embankment dams. In general, there is no systematic study of the comparison of the responses due to all reference axes with responses due to critical direction (critical responses). The main objective of this paper is to investigate the response of embankment dams due to Sarpol-e Zahab earthquake records. This investigation carried out with different incident angles and regarding different reference axes. For this purpose, all existing embankment dams at a distance of 100 km from the earthquake epicenter were identified and a typical dam of the region was selected for a case study. In the next step, the embankment dam responses subjected to rotated ground motion accelerations as well as all reference axes directions were investigated. The results showed that, in general, reference axes directions did not always lead to the maximum responses and it is necessary to perform parametric analysis with different incident angle of accelerations to obtain critical responses.

2. Ground Motion Records Used and Numerical Modeling of the Embankment Dams

2.1. Ground Motion Input

On November 12, 2017, a devastating earthquake with a moment magnitude of 7.3 struck off the east province of Iran, at coordinates of 34.88 degrees North latitude and 45.84 degrees East longitude. The epicenter was 10 kilometers from Ezgeleh and about 37 kilometers northwest of Sarpol-e Zahab city of Kermanshah province, located on the border of Iran-Iraq [35].

The Sarpol-e Zahab earthquake were recorded at 110 stations by the accelerographs of Iran Strong Motion Network (ISMN). Among these, uncorrected ground motion accelerations are available at 90 stations through the building and housing research center (BHRC) [36]. Figure (1) shows all stations located within 200 km from the earthquake epicenter. In this figure, the asterisk indicates earthquake epicenter, the solid line indicates causative fault trace, circles represent recording stations, and their size is proportional to the peak ground acceleration at the station. According to the figure, highest values of PGA has been recorded at Sarpol-e Zahab (SPZ), Kerend (KRD), and Goorsefid (GRS) stations, toward which the rupture propagates.

The ground motions with maximum acceleration less than 200 cm/s^2 do not have much effect on

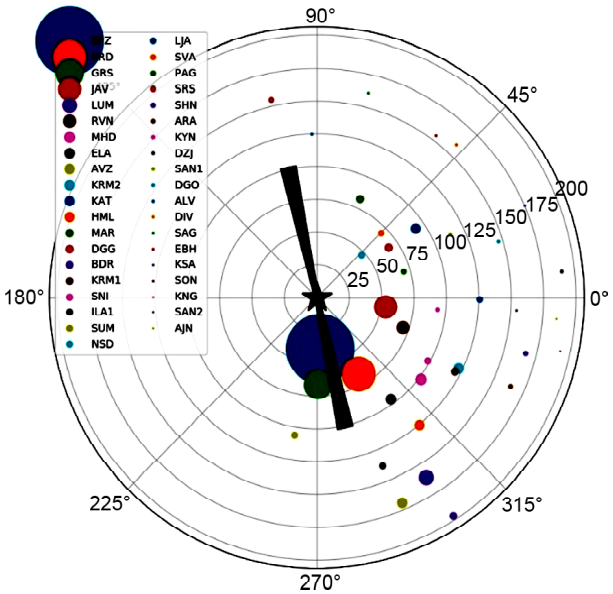

Figure 1. All recording stations located within 200 km from the earthquake epicenter (asterisk: Earthquake epicenter, Solid line: Fault trace, Circles: Recording stations, Circle Size: Maximum Acceleration at the Station).

Table 1. Stations with maximum acceleration greater than 200 cm/s^2.

Station Code	Station Name	Epicentral Distance (km)	Station Latitude	Station Longitude	Transverse Component Angle	PGA (cm/s^2)	Station Vs (m/s)
SPZ	Sarpol-e Zahab	39.034	34.460	45.870	90	645	619
KRD	Kerend	66.190	34.280	46.240	90	315	800
GRS	Goorsefid	65.925	34.220	45.850	90	262	403
JAV	Javanrood	53.069	34.810	46.490	90	208	298

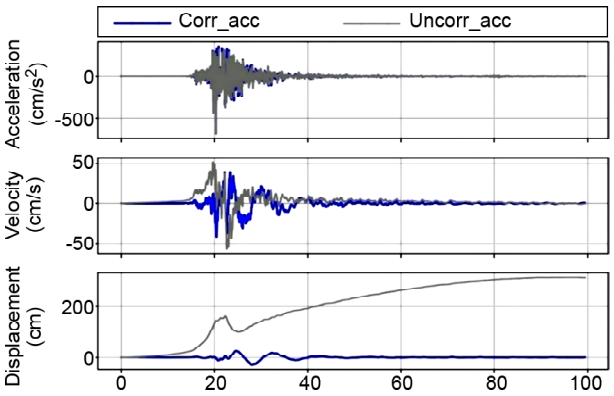

Figure 2. Acceleration, velocity, and displacement time history of corrected and uncorrected motion of longitudinal component at SPZ station.

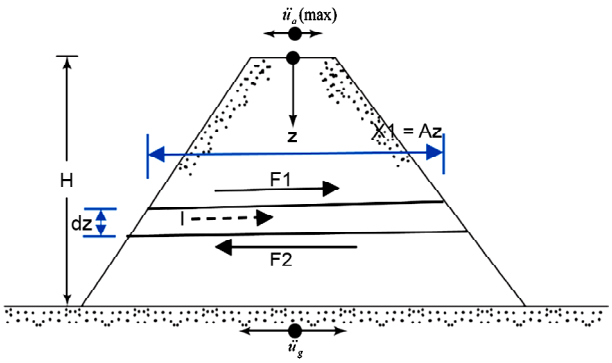

Figure 3. Shear beam method for evaluation of maximum crest acceleration [38].

structures. Therefore, by checking the recorded acceleration at all stations, the records with a maximum acceleration greater than 200 cm/s^2 are extracted and listed in Table (1).

Selected ground motion records are filtered with a fifth-order Butterworth bandpass filter from 0.1-25 Hz, and then the baseline corrections are applied. Figure (2) shows acceleration, velocity and displacement time histories of corrected and uncorrected motion of longitudinal component at Sarpol-e Zahab (SPZ) station. Although the epicentral distance of SPZ station is greater than 20 km, denoising of velocity time history by wavelet transform unfolds the distinct velocity pulse [37]. By considering a distinct peak in the acceleration response spectrum at the period of 1 second, it can be claimed that the Sarpol-e Zahab record has the characteristics of the near-fault earthquake.

2.2. Numerical Modeling of Embankment Dams

Due to a large number of time history analyses and regarding that this type of analysis is time-consuming, a shear beam model was used for numerical modeling of dams. In accordance with Figure (3), the governing differential equation of the dams excited by the ground motion can be extracted as follows [38]:

$$\frac{\partial^2 u}{\partial t^2}-\frac{G}{\rho}\left[\frac{\partial^2 u}{\partial z^2}+\frac{1}{z}\frac{\partial u}{\partial z}\right]=-\frac{\partial^2 u_g}{\partial t^2} \tag{1}$$

By solving this differential equation, the relative displacement at the height of the dam can be derived as follows.

$$u(z,t)= \sum_{n=1}^{n=\infty}\frac{2J_0\left[\beta_n(z/H)\right]}{\omega_n\beta_n J_1(\beta_n)}\int_0^t \ddot{u}_g \sin\left[\omega_n(t-t')\right]dt' \tag{2}$$

where J_0 and J_1 are Bessel functions, β_n is the zero value of the frequency function $\left(J_0\left(\omega_n H\times\sqrt{\frac{\rho}{G}}\right)=0\right)$ and ω_n is the undamped natural frequency of the dam $\left(\frac{\beta_n}{H}\times\sqrt{\frac{G}{\rho}}\right)$. By solving Equation (2), relative displacement at the height of the dam is obtained, then velocity and acceleration can be found by performing differentiation. In order to obtain absolute responses, the ground motion must be added up to the relative responses of the dam.

For considering nonlinear behavior of soils, an equivalent linear method (ELM) has been used. This method can approximately simulate the actual stress-strain path during cyclic loading by using

modulus reduction and damping curves. The modules reduction and damping curves are derived from Darendeli general relationships [39]. Using a hyperbolic model and conducting multiple experiments on various soil types, Darendeli suggested the following relationships and coefficients.

$$\frac{G}{G_{\max}} = \frac{1}{1+\left(\frac{\gamma}{\gamma_r}\right)^a} \tag{3}$$

$$D_{Adjusted} = b \times \left(\frac{G}{G_{\max}}\right)^{0.1} \times D_{Ma\sin g} + D_{\min} \tag{4}$$

where γ_r indicates reference strain (%), *a* is curvature coefficient, Dmin stands for small-strain material damping ratio (%), *b* is scaling coefficient, and $D_{Adjusted}$ is scaled and capped material damping (%). All unknown parameters of the model are computed using parametric analysis. Effective average shear strain and average confining stresses are utilized in the iterative process of equivalent linear approach.

2.3. Shear Beam (SB) Model Validation

The shear beam model captures the most important aspects of various 2D dynamic response problems without the computational cost and complexity of dynamic finite element analyses. The applicability and accuracy of this approach have been investigated by many researchers [40-42]. The validity of the shear beam model is examined by comparing the results obtained from this model with those of finite element (FE) analyses. In this regard, one of the dams (dam type B) introduced by Dakoulas and Gazetas [42] excited by Eureka record (1954) is selected. Figure (4) shows the maximum crest displacements obtained from shear beam model used in this study (solid line) and those of FE analyses. This figure shows that the performance of shear beam model is quite satisfactory.

3. The Orientation of the Reference Axes for Sarpol-e Zahab Earthquake Records

3.1. Principal Direction

According to the Penzien and Watabe [16], principal directions of all recorded ground motions have been computed. Moving window approach and optimization rule have been used to calculate these

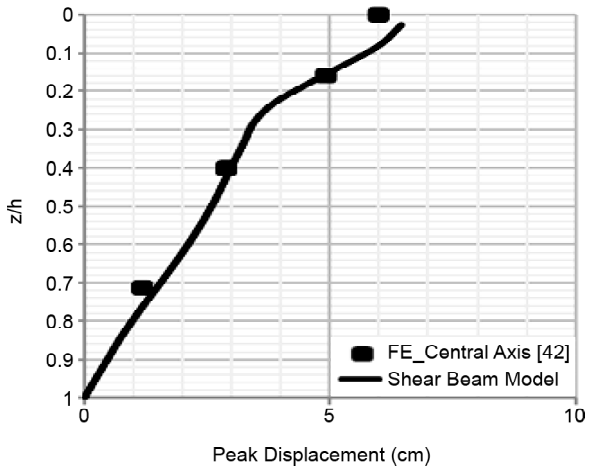

Figure 4. Distribution of maximum crest displacement with depth from SB and FE analyses.

Table 2. All reference axes directions for four selected ground motions.

Reference Axis	SPZ (Degree)	KRD (Degree)	GRS (Degree)	JAV (Degree)
As_Recorded	0.00	0.00	0.00	0.00
FN/FP	190.00	10.00	190.00	10.00
GMRotI50_acc	56.00	43.00	51.00	52.00
GMRotI50_vel	56.00	50.00	21.00	87.00
GMRotI50_dis	22.00	22.00	22.00	22.00
GMRotI86_acc	62.00	40.00	50.00	56.00
GMRotI86_vel	70.00	47.00	50.00	63.00
GMRotI86_dis	6.00	6.00	6.00	6.00
PD_win_3 sec	302.43	298.81	36.01	271.26
PD_win_5 sec	207.24	236.66	230.97	158.32
PD_win_7 sec	172.48	155.83	193.78	298.57
PD_win_9 sec	340.53	164.93	47.23	307.18
MSD_T=1 sec	121.83	18.45	166.85	272.17

directions. Regarding that calculated variance of each component depends on the length of the moving window, four different window lengths have been utilized. Results for a various window length of 3, 5, 7, and 9 seconds have been reported in Table (2). For example, "PD_win_7 sec" stands for the principal direction of each ground motion record with moving window of 7-second length. All 90 as-recorded motions have been rotated to principal directions and depicted as arrows on the map. Scanning this map reveals that these directions do not point toward earthquake epicenter.

3.2. GMRotIpp

The direction independent of sensor orientation and oscillator period is defined as GMRotIpp. On

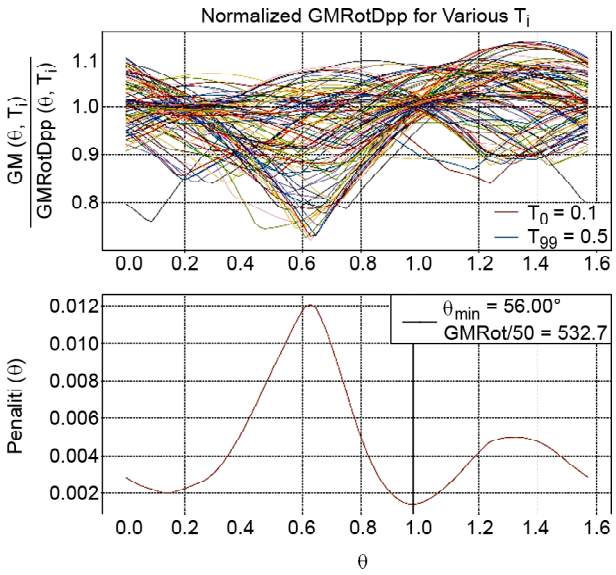

Figure 5. Median value (pp =50) and direction of GMRotI50 for maximum oscillator period of 5 second and acceleration response of SPZ ground motion.

the basis of research done by Boore et al. [31] this direction is sensitive to considered maximum oscillator period. Therefore, in present research not only this issue has been investigated, but also the different types of responses (acceleration, velocity, displacement) and statistical percent percentile (pp) have been regarded. Figure (5) shows the median value (pp=50) and direction of GMRotI50 for maximum oscillator period of 5 second and acceleration response of SPZ ground motion. Table (2) shows GMRotIpp for percent percentile of 50 and 86 and for different response types.

3.3. MSD

According to Huang et al. [33-34], directions of maximum spectral demand have been computed for all selected ground motions. MSD direction and value depends not only on the period of SDOF system, but also on the response type. Therefore, it is important to choose a proper period of structure for which the MSD direction is computed. In this paper, for linear analysis predominant period of linear system and for equivalent linear analysis predominant period of both linear and equivalent linear system have been used. Figure (6) shows MSD values and directions for all selected ground motions at predominant period of 1 second. As can be seen from Figure (6), there is a distinct directionality in SPZ ground motion record at the period of 1 second. This issue can be inferred as

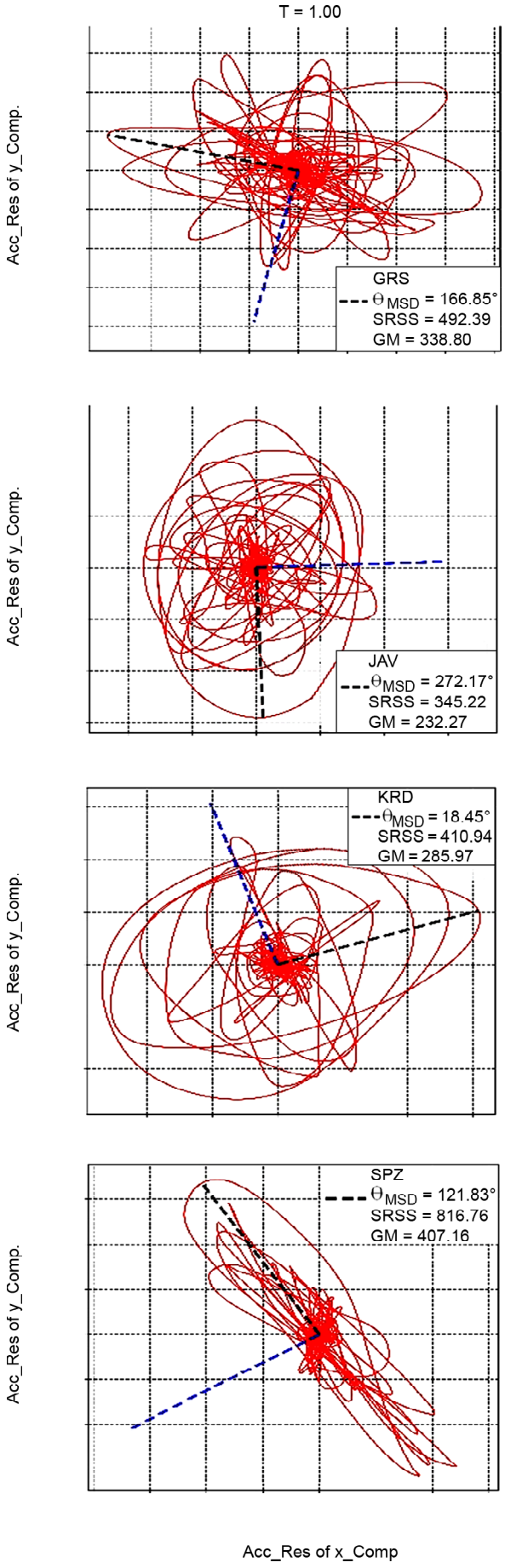

Figure 6. Directions and values of maximum spectral demand for all selected ground motions (SPZ, KRD, GRS, and JAV).

near-fault earthquake characteristic.

On the basis of reconnaissance report of IIEES the causative fault strike is approximately North 10 degrees West (N10W) [35]. Therefore, according to the aforementioned definitions, reference axes directions have been computed for all selected ground motion records and reported in Table (2).

4. Results and Discussions

4.1. Response Spectra of all Directions

All selected ground motion records, in addition to the reference axes directions, are rotated by different angles in the range of 0 to 360 degrees. Then response spectra are constructed for each individual component and geometric mean (GM), as well as the square root of the sum of the squares (SRSS) of two horizontal components, are calculated. According to the shear wave velocity at each recording station and seismic hazard zoning map of Iran National Standard No. 2800, design-based earthquake (DBE) spectrum is constructed for each recording station site [43].

Figure (7) shows all constructed response spectra of different directions and reference axes for transverse component of SPZ ground motion record. It is clear from this figure that the MSD spectrum is envelope of all spectra and is conservatively used in ASCE/SEI 41 standard. Besides, distinct differences of Standard No. 2800 spectrum with SPZ acceleration response spectra are shown in this figure. These differences are much more noticeable in the constant acceleration region and period of 1 second. The considerable diversity at the period of 1 second can be attributed to the ground motion directionality. Regarding existing building structures in the earthquake-affected region, which are usually low and mid-rise structures (short periods), design forces based on the Standard No. 2800 spectrum are less than seismic demands. The observed damages of buildings reflect this issue.

For each period in response spectra (T_1, T_2, … in Figure 7), standard deviation of maximum responses due to all directions have been computed. These calculations eventuate in standard deviation spectrum for x-component of SPZ ground motion record (SPZ_x spectrum). Averaging of this spectrum in the period range of 0 to 2 second leads to the average standard deviation of SPZ x-component (SPZ_x). This procedure has been repeated for GM and SRSS spectrum of SPZ record and denoted as SPZ-GM and SPZ-SRSS respectively. Accordingly, the average standard deviations for three other records are calculated and has been shown in Figure (8). The results that can be inferred from this figure are as follows:

- The geometric mean spectrum has the minimum standard deviation and consequently the least variation.
- The individual component spectrum has the most variation.
- SPZ ground motion record spectra show the most variation.

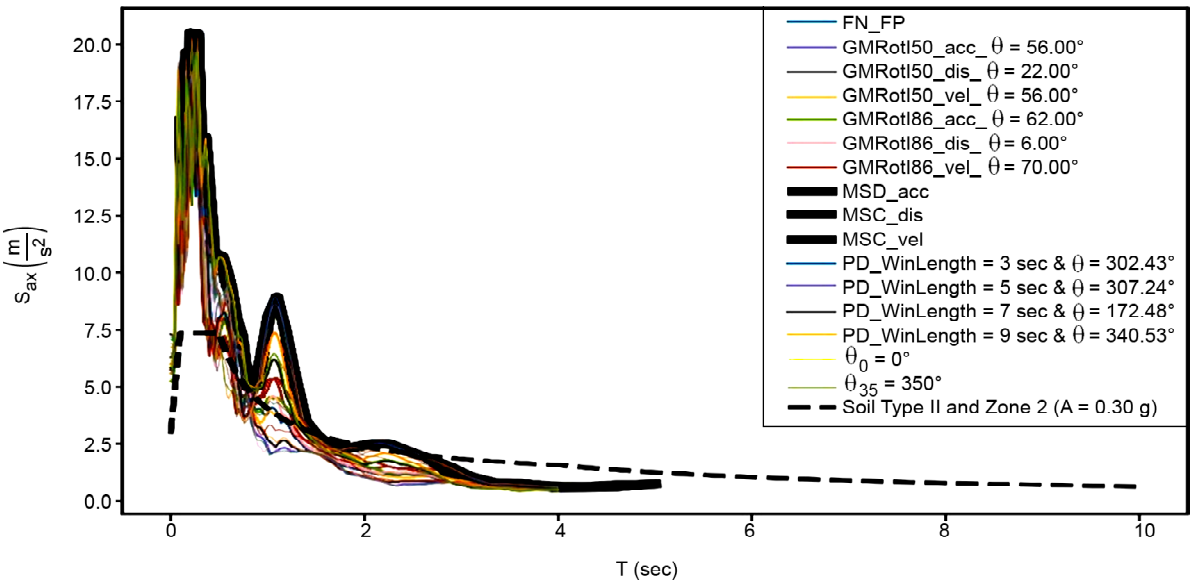

Figure 7. Constructed response spectra of different directions and reference axes for transverse component of SPZ ground motion record.

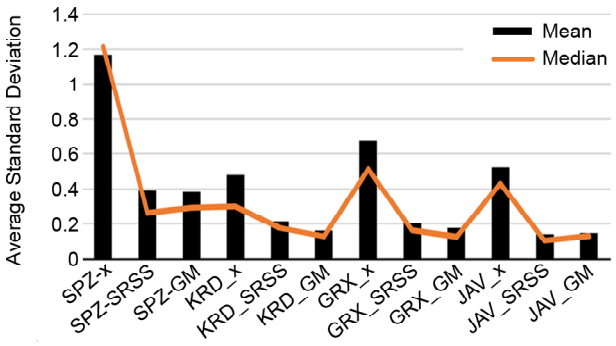

Figure 8. Average standard deviation of maximum responses due to various directions at oscillator period in range of 0 to 2 second.

4.2. Parametric Study to Determine Critical Responses and Directions

All embankment dams within radii of 100 km from the earthquake epicenter have been reconnoitered and a typical embankment dam with height of 60 m has been selected as a case study. Table (3) shows some important characteristics of the dam.

According to the aforementioned process, numerical modeling of the embankment dam has been developed using the Python programming language. To investigate the effect of ground motion directions on the response of the embankment dam, numerous parametric analyses have been carried out. In order to perform these analyses, as-recorded ground motions are rotated to different angles in the range of 0-360 degrees in 10 degree steps. For each selected recording station, these 35 different directions as well as all 14 above-mentioned reference axes directions, added up to form an acceleration seed. Then linear and equivalent linear analyses of the dam are performed using each individual component of the acceleration seed. This process is repeated for all selected recording stations then acceleration, velocity, and displacement responses of the dam crest are computed. Figure (9) shows maximum crest velocities and accelerations of the dam due to four selected ground motion records with different incident angles in the equivalent linear model. In this figure, solid lines show responses due to different orientation of records (0-360°, 10° steps), and asterisks indicate responses of reference axes directions. As can be seen from this figure, the orientation associated with the maximum responses do not coincide with reference axes directions. Moreover, this figure clarifies that critical directions depend on the input ground motion and response type. Therefore, for the specified ground motion record different responses result in different critical orientations.

Table 3. Characteristics of the dam used.

Height	Average Density (KN/m3)	Average G (Kpa)	Ccore/Cshell	h/H	Inhomogeneity(m)	T1
60	20	300000	1	0	0	0.4

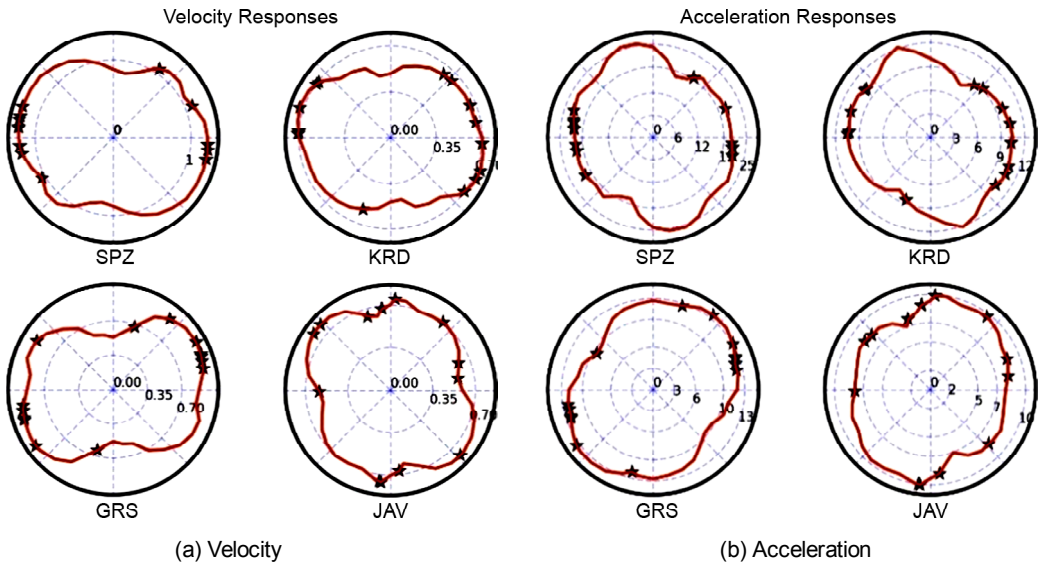

Figure 9. Maximum crest responses of the dam subjected to records with different incident angles (solid lines show all orientations and asterisks show reference axes directions.

Figure (10) shows maximum crest accelerations of the dam due to SPZ ground motion with different incident angles in the equivalent linear model. As can be seen from this figure, none of the reference axes directions has led to the critical response. Comparison of critical responses for all recording stations, indicated by "max", with responses due to different reference axes directions in the equivalent linear analysis is illustrated in Figure (11). Furthermore, Figure (12) shows maximum crest accelerations of the dam subjected to all selected ground motions with different incident angles. In this figure, triangular markers indicate responses due to reference axis directions and dotted-lines denote median values.

As can be seen from Figures (11) and (12), although maximum acceleration of KRD as-recorded motion is greater than GRS motion, maximum and mean value response of GRS is greater than KRD. By investigating different responses, including displacement, velocity, and acceleration, due to linear and equivalent linear analyses, the important outcomes can be summarized as follows:

- Regarding only as-recorded motions almost al ways underestimate responses.
- Generally, critical responses occur at directions other than reference axis directions.

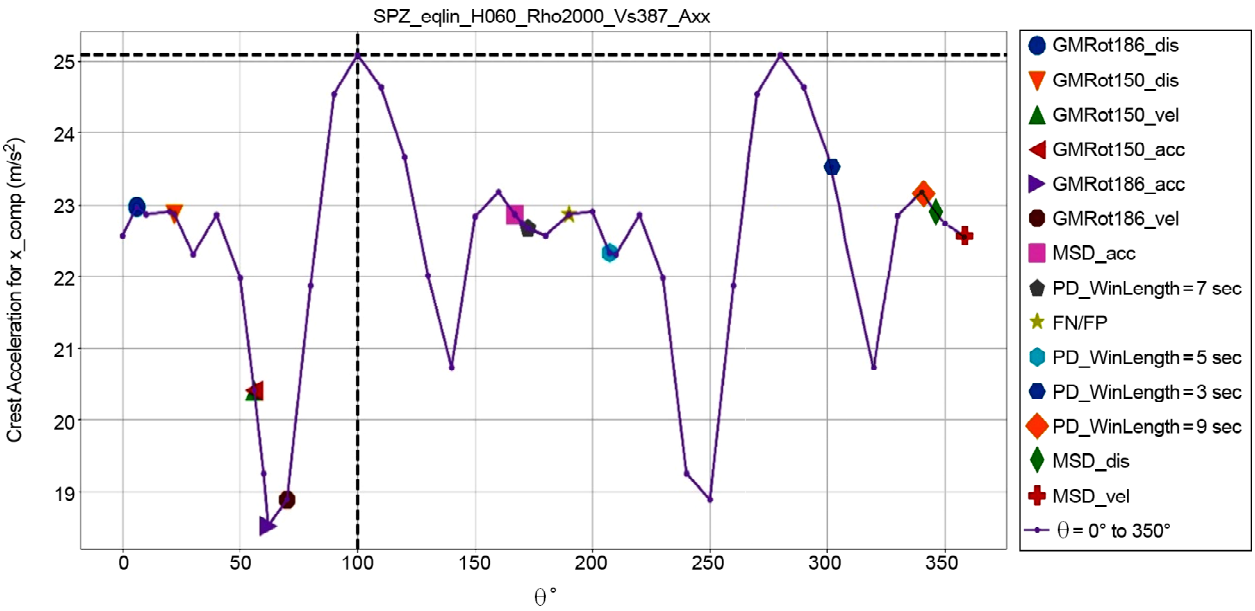

Figure 10. Maximum crest accelerations of the dam subjected to SPZ ground motion with different incident angles (equivalent linear analysis).

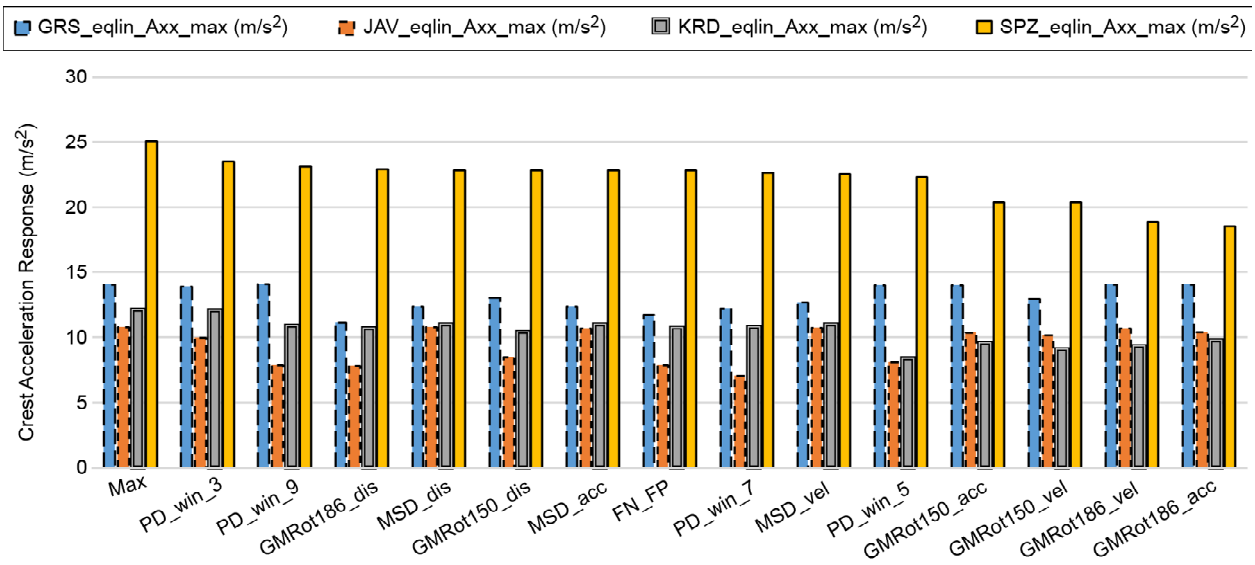

Figure 11. Comparison of critical responses for all recording stations (max) with responses due to different reference axes (equivalent linear analysis).

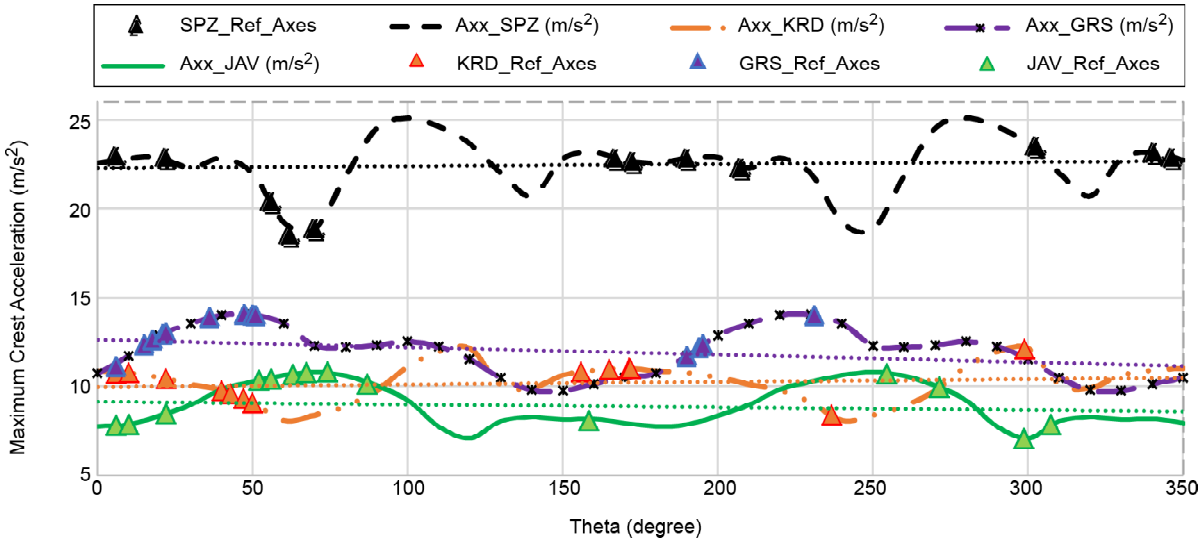

Figure 12. Maximum crest accelerations of the dam subjected to all selected ground motions with different incident angles (equivalent linear analysis).

- Critical directions obtained from linear models do not coincide with those of equivalent linear models.
- Different response types lead to different critical directions.
- Although response spectrum of MSD direction is the envelope of all directions, time history analysis due to this direction does not lead to the critical response.

5. Conclusion

The main objective of this research is to investigate the effects of a different incident angle of ground motions on the responses of a typical embankment dam. There are different ground motion reference axes recommended by codes and researchers. In order to evaluate the applicability of these recommended reference directions, numerous time history analysis of the embankment dam with different incident angles of Sarpol-e Zahab earthquake records were performed. The comparison of these results with those of reference axes directions showed that, generally, the critical directions are not coincident with reference axes directions. The investigations also revealed that the critical directions depend on the considered EDP. For instance, the critical direction of the maximum crest velocity excited by SPZ record is 175 degrees, while the same direction of the maximum crest acceleration is 100 degrees. In addition, the critical directions also depend on the input ground motions. In some cases, in comparison with the critical responses, the derived results of the recommended directions have been underestimated by about 30 percent. Therefore, a parametric study with regarding all non-redundant directions is essential to find the maximum desired EDPs.

References

1. Newmark, N.M. (1975) Seismic design criteria for structures and facilities, Trans-Alaska pipeline system. *Proceedings of the US National Conference on Earthquake Engineering*.

2. Rosenblueth, E. and Contreras, H. (1977) Approximate design for multicomponent earthquakes. *Journal of the Engineering Mechanics Division*, **103**(5), 881-893.

3. Wilson, E.L., Suharwardy, I., and Habibullah, A. (1995) A clarification of the orthogonal effects in a three-dimensional seismic analysis. *Earthquake Spectra*, **11**(4), 659-666.

4. Menun, C. and Kiureghian, A.D. (1998) A replacement for the 30%, 40%, and SRSS rules for multicomponent seismic analysis. *Earthquake Spectra*, **14**(1), 153-163.

5. Lopez, O.A., Chopra, A.K., and Hernandez, J.J. (2001) Evaluation of combination rules for maximum response calculation in multicomponent seismic analysis. *Earthquake Engineering & Structural Dynamics*, **30**(9), 1379-1398.

6. Marinilli, A. and Lopez, O.A. (2008) Evaluation of critical responses and critical incidence angles obtained with RSA and RHA. *The 14th World Conference on Earthquake Engineering*, Beijing, China.

7. Athanatopoulou, A. (2005) Critical orientation of three correlated seismic components. *Engineering Structures*, **27**(2), 301-312.

8. Rigato, A.B. and Medina, R.A. (2007) Influence of angle of incidence on seismic demands for inelastic single-storey structures subjected to bi-directional ground motions. *Engineering Structures*, **29**(10), 2593-2601.

9. Hariri-Ardebili, M. and Saouma, V. (2014) Impact of near-fault vs. far-field ground motions on the seismic response of an arch dam with respect to foundation type. *Dam Eng.*, **24**(1), 19-52.

10. Fontara, I.K.M., Kostinakis, K.G., Manoukas, G.E., and Athanatopoulou, A.M. (2015) Parameters affecting the seismic response of buildings under bi-directional excitation. *Struct. Eng. Mech.*, **53**(5), 957-979.

11. Mitropoulou, C.C. and Lagaros, N. (2016) Critical incident angle for the minimum cost design of low, mid and high-rise steel and reinforced concrete-composite buildings. *Int. J. Optim. Civil Eng.*, **6**(1), 135-158.

12. Kostinakis, K.G., Manoukas, G.E., and Athanatopoulou, A.M. (2017) Influence of seismic incident angle on response of symmetric in plan buildings. *KSCE Journal of Civi Engineering*, 1-11.

13. Roy, A., Santra, A., and Roy, R. (2018) Estimating seismic response under bi-directional shaking per uni-directional analysis: Identification of preferred angle of incidence. *Soil Dynamics and Earthquake Engineering*, **106**, 163-181.

14. Bozorgnia, Y., Abrahamson, N.A., Atik, L.A., Ancheta, T.D., Atkinson, G.M., Baker, J.W., ... and Darragh, R. (2014) NGA-West2 research project. *Earthquake Spectra*, **30**(3), 973-987.

15. ASCE/SEI (2016) *Minimum Design Loads for Buildings and other Structures*. ASCE/SEI 7-16, Reston, VA.

16. Penzien, J. and Watabe, M. (1974) Characteristics of 3-dimensional earthquake ground motions. *Earthquake Engineering and Structural Dynamics*, **3**(4), 365-373.

17. Kubo, T. and Penzien, J. (1979) Analysis of three-dimensional strong ground motions along principal axes, San Fernando earthquake. *Earthquake Engineering and Structural Dynamics*, **7**(3), 265-278.

18. Kubo, T. and Penzien, J. (1979) Simulation of three-dimensional strong ground motions along principal axes, San Fernando earthquake. *Earthquake Engineering and Structural Dynamics*, **7**(3), 279-294.

19. Reyes, J. and Kalkan, E. (2012) Relevance of fault-normal/parallel and maximum direction rotated ground motions on nonlinear behavior of multi-story buildings. *Proceedings of the 15th World Conference on Earthquake Engineering*.

20. Stewart, J.P., Chiou, S.J., Bray, J.D., Graves, R.W., Somerville, P.G., and Abrahamson, N.A. (2002) *Ground Motion Evaluation Procedures for Performance-Based Design, in PEER Report 2001/09*. University of California, Berkeley: Pacific Earthquake Engineering Research Center.

21. Mavroeidis, G.P. and Papageorgiou, A.S. (2003) A mathematical representation of near-fault ground motions. *Bulletin of the Seismological Society of America*, **93**(3), 1099-1131.

22. Maniatakis, C.A., Taflampas, I., and Spyrakos, C. (2008) Identification of near-fault earthquake record characteristics. *The 14th World Conference on Earthquake Engineering*, Beijing, China.

23. Somerville, P.G. (2005) Engineering characterization of near fault ground motions. *Proc., NZSEE 2005 Conference*.

24. Somerville, P. and Graves, R. (1993) Conditions that give rise to unusually large long period ground motions. *The Structural Design of Tall*

Buildings, **2**(3), 211-232.

25. Somerville, P.G. (2002) Characterizing near fault ground motion for the design and evaluation of bridges. *Third National Conference and Workshop on Bridges and Highways*, Portland, Oregon.

26. Bray, J.D. and Rodriguez-Marek, A. (2004) Characterization of forward-directivity ground motions in the near-fault region. *Soil Dynamics and Earthquake Engineering*, **24**(11), 815-828.

27. Lu, Y. and Panagiotou, M. (2014) *Characterization and Representation of Pulse-like Ground Motions Using Wavelet-Based Cumulative Pulse Extraction*.

28. Kalkan, E. and Kwong, N.S. (2013) Pros and cons of rotating ground motion records to fault-normal/parallel directions for response history analysis of buildings. *Journal of Structural Engineering*, **140**(3), 04013062.

29. Davoodi, M., Jafari, M.K., and Hadiani, N. (2013) Seismic response of embankment dams under near-fault and far-field ground motion excitation. *Engineering Geology*, **158**, 66-76.

30. Hadiani, N., Davoodi, M., and Jafari, M. (2013) Correlation between settlement of embankment dams and ground motion intensity indices of pulse-like records. *Iranian Journal of Science and Technology. Transactions of Civil Engineering*, **37**(C1), 111.

31. Boore, D.M., Watson-Lamprey, J., and Abrahamson, N.A. (2006). Orientation-independent measures of ground motion. *Bulletin of the seismological Society of America*, **96**(4A), 1502-1511.

32. Baker, J.W., and Cornell, C.A. (2006). Which spectral acceleration are you using? *Earthquake Spectra*, **22**(2), 293-312.

33. Huang, Y.-N., Whittaker, A.S., and Luco, N. (2008) Maximum spectral demands in the near-fault region. *Earthquake Spectra*, **24**(1), 319-341.

34. Huang, Y.-N., Whittaker, A.S., and Luco, N. (2009) Orientation of maximum spectral demand in the near-fault region. *Earthquake Spectra*, **25**(3), 707-717.

35. IIEES (2017) *Preliminary Report of Mw7.3 Sarpol-e Zahab Earthquake on November 12, 2017*. 5th Edition, Tehran, Iran.

36. http://smd.bhrc.ac.ir/Portal/fa/FastDownload. Road, Housing and Urban Research Center (BHRC), (2017).

37. Lee, G., Wasilewski, F., Gommers, R., Wohlfahrt, K., O'Leary, A., and Nahrstaedt, H. (2006) PyWavelets - Wavelet Transforms in Python, https://github.com/PyWavelets/pywt [Online; accessed 2018-MM-DD].

38. Das, B. and Ramana, G. (2010) *Principles of Soil Dynamics*, 2nd Edn. Cengage Learning. Inc, Boston.

39. Darendeli, M.B. (2001) Development of a New Family of Normalized Modulus Reduction and Material Damping Curves.

40. Gunturi, V.R. and Elgamal, A.-W. (1998) A class of inhomogeneous shear models for seismic analysis of landfills. *Soil Dynamics and Earthquake Engineering*, **17**(3), 197-209.

41. Gazetas, G. (1987) Seismic response of earth dams: some recent developments. *Soil Dynamics and Earthquake Engineering*, **6**(1), 2-47.

42. Dakoulas, P. and Gazetas, G. (1985) A class of inhomogeneous shear models for seismic response of dams and embankments. *International Journal of Soil Dynamics and Earthquake Engineering*, **4**(4), 166-182.

43. BHRC (2014) *Iranian Code of Practice for Seismic Resistant Design of Buildings*. 4th Edition, Road, Housing and Urban Research Center, Tehran, Iran.